23rd International Congress on Sound & Vibration
Athens, Greece 10-14 July 2016
ICSV23

NUMERICAL ESTIMATION OF THE ABSORPTION COEFFICIENT OF FLEXIBLE MICRO-PERFORATED PLATES IN AN IMPEDANCE TUBE

Muttalip Aşkın Temiz
Eindhoven University of Technology, Dept. of Mechanical Engineering, Eindhoven, The Netherlands
e-mail: m.a.temiz@tue.nl

Jonathan Tournadre
KU Leuven, Dept. of Mechanical Engineering, Celestijnlaan 300B, 3001 Leuven, Belgium

Ines Lopez Arteaga
Eindhoven University of Technology, Dept. of Mechanical Engineering, Eindhoven, The Netherlands
KTH Royal Institute of Technology, Dept. of Aeronautical and Vehicle Engineering, Stockholm, Sweden

Paula Martínez-Lera
Siemens Industry Software, Researchpark 1237, Interleuvenlaan 68, 3001 Leuven, Belgium

and Avraham Hirschberg
Eindhoven University of Technology, Dept. of Applied Physics, Eindhoven, The Netherlands

In this study, we numerically model a vibro-acoustic system consisting of a flexible micro-perforated plate (f-MPP) and an acoustic medium. Combined with a back-cavity, micro-perforated plates are considered as a promising noise control technology due to their tunable, wide-band sound absorption characteristics and robust performance. An MPP consists of a plate with uniformly distributed perforations whose diameters are in the order of a millimeter. These perforations are small enough to dissipate the acoustic perturbations due to the viscous effects caused by the presence of the Stokes layers. When the plate is rigid, the sound dissipation mechanism for a specific frequency bandwidth is determined by the perforation diameter, plate thickness, plate porosity and the back cavity depth. Yet, when the plate is flexible, additional absorption peaks, which cannot be determined by the parameters mentioned before, are observed in the measurements. This phenomenon is due to the vibro-acoustic coupling of the flexible plate and the acoustic medium. To model the vibro-acoustic system numerically, we couple two 3D cylindrical acoustic mediums, i.e. incident and back cavity regions, with a flexible plate consisting of shell elements. The perforations are separately located on the plate as independent transfer admittance elements with impedance values obtained from existing models. The system is disturbed with a plane wave excitation and the assessment of the model is done by comparing the calculated absorption coefficient with the experimental results from the literature. In the future, we plan to investigate the effect of perforation positions with the help of the model built in this study.

1. Introduction

Micro-perforated plates (MPPs) have been a popular subject in acoustics since their high potential in sound absorption was pointed out by Maa [1]. MPPs are plates with very small perforations that are used for absorbing sound when utilized with a back-cavity. Although this configuration is quite similar to Helmholtz resonators, the size of the perforations causes viscous dissipation and increases

the absorption bandwidth compared to purely reactive sound absorbers. In our previous studies, we have investigated the effect of perforation geometry [2] and non-linearity [3].

Another reason for MPPs becoming popular recently is the fact that they can be produced from a large number of materials. In some cases, the size of the plate and material properties lead to a vibro-acoustic system. These effects have been noticed by Lee and Swenson first, as an additional absorption peak [4]. The first attempt to model this vibro-acoustic coupling effect in MPPs is performed by Lee *et al.* [5]. They propose a theoretical model to capture the vibro-acoustic effects on the sound absorption for a rectangular, finite flexible micro-perforated plate (f-MPP). They use Maa's transfer impedance definition and couple the particle velocity with plate vibrations after a modal analysis. Toyoda *et al.* follow a similar procedure to the one used by Lee *et al.* in order to estimate the absorption coefficient for circular f-MPPs [6]. Additionally, they discuss the effect of surface impedance of the plate in absorption. They compare their model with impedance tube measurements. Zheng *et al.* use the knowledge of f-MPPs to design a hybrid passive-active noise control system and have verified their model with experiments [7]. Furthermore, Bravo *et al.* analyse a more complicated case. In their study not only the MPP, but also the back wall of the back cavity is flexible [8]. They propose an analytical model for this fully coupled system, which is validated by experiments. Later on, Bravo *et al.* propose a fully coupled modal model for multiple layers of f-MPPs to optimize the sound absorption [9]. They have tested this model for a 2-layer f-MPP configuration. Quite recently, Li *et al.* have investigated the effect of the perforation position on a f-MPP [10]. To do that, they redefine the transfer impedance definition as a function of perforation position on the plate.

Although all of the above mentioned approaches are inspirational, they are valid for uniformly distributed perforations, except for Li *et al.* [10], which requires re-calculation of the transfer impedance for each perforation and plate mode separately. To be able to investigate the perforation distribution and optimize it, the need for a versatile and efficient tool is present.

In this study, we propose a numerical model which takes the positions of the perforations into account even though they are not distributed uniformly. To do that, we consider an impedance tube configuration and calculate the absorption coefficient of the f-MPP backed by a cavity (see Figure 1a). The model solves the Helmholtz equation for the acoustic medium and the f-MPP is represented as a shell on which the perforations are defined by transfer impedance boundary condition. We have verified the model with previous results from the literature and we obtain good agreement in both purely acoustic and vibro-acoustic cases.

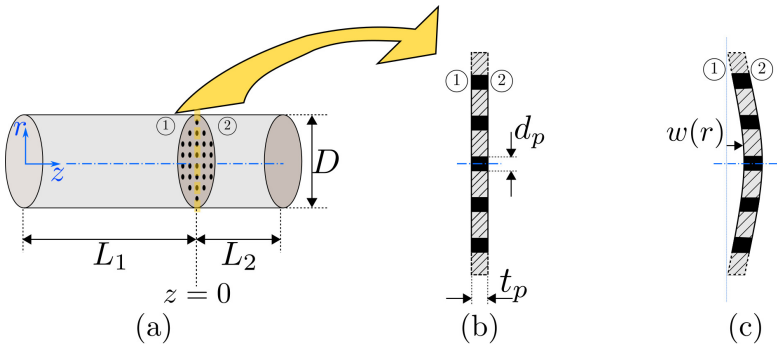

Figure 1: (a) Impedance Tube configuration: ① tube domain, ② back-cavity domain; (b) Cross-section of the MPP (zoomed); (c) Cross-section of the f-MPP (zoomed).

2. Theoretical Background

Assuming harmonic plane waves and neglecting the thermal and viscous effects in the acoustic mediums ① and ② shown in Figure 1-a, the wave equation in frequency domain is given by the

Helmholtz equation [11]

$$\omega^2 \hat{p}_n(z) + c_0^2 \nabla^2 \hat{p}_n(z) = 0, \tag{1}$$

where $\omega = 2\pi f$ is the radial frequency, c_0 is the speed of sound, ∇^2 is the *Laplacian* operator, and $\hat{p}_n$ is the acoustic pressure in medium ⓝ.

The flexible MPP is assumed to be a thin, homogeneous plate (Figure 1c) whose equation of motion is given by [12]:

$$D_p \nabla^2 \nabla^2 w(r) - \rho_p t_p \omega^2 w(r) = \hat{F}. \tag{2}$$

In Eq. (2), ρ_p is the density, $w(r)$ is the displacement of the MPP; $\hat{F}$ is the external point force acting on the plate surface; $D_p = E(1 + j\eta)t_p^3/[12(1-\nu^2)]$ is the flexural rigidity where E is the Young's modulus, η is the loss factor, $j = \sqrt{-1}$ is the imaginary number and ν is the Poisson ratio of the MPP material.

In case of rigid MPP, the acoustic mediums ① and ② are connected through the micro-perforations that are defined by perforation diameter d_p, and plate thickness t_p, in Figure 1b. This relation is expressed as the acoustic transfer impedance for a single perforation Z_t, and given by [1]

$$Z_t = \frac{\Delta\hat{p}}{\hat{u_p}} = j\omega t_p \rho_0 \left[1 - \frac{2}{Sh\sqrt{-j}} \frac{J_1(Sh\sqrt{-j})}{J_0(Sh\sqrt{-j})}\right]^{-1} + 2\alpha R_s + j\delta\omega\rho_0 \frac{d_p}{2}, \tag{3}$$

where $\Delta\hat{p} = \hat{p}_1 - \hat{p}_2$ is the acoustic pressure difference across the MPP, $\hat{u}_p$ is the acoustic particle velocity in a perforation, ρ_0 is the density of the acoustic medium, J_n is the Bessel function of the first kind of order n, $Sh = d_p\sqrt{\omega\rho_0/(4\mu)}$ is the Shear number where μ is the dynamic viscosity of the acoustic medium; $(2\alpha R_s)$ and $(j\delta\omega d_p/2)$ are the resistive and reactive end-corrections where $R_s = 0.5\sqrt{2\mu\rho_0\omega}$ is the surface resistance, and α and δ are the resistive and reactive end-correction coefficients, respectively.

Provided that the perforations are uniformly distributed and far enough from each other, the porosity, σ, is also required to calculate the transfer impedance of the entire plate, $Z_T = Z_t/\sigma$ [1].

Assuming that the flexible plate is infinitely thin, the vibro-acoustic coupling of the f-MPP and the acoustic mediums is performed using the following relations:

$$\hat{F} = \hat{p}_1(0^-) - \hat{p}_2(0^+), \tag{4a}$$

$$\hat{u}_{1,2}(r, 0) = j\omega w(r), \tag{4b}$$

on the plate surface.

We evaluate the acoustic performance of the model by calculating the absorption coefficient $\beta = 1 - |(\hat{p}^-/\hat{p}^+)_1|^2$, where $\hat{p}^+$ and $\hat{p}^-$ are the complex amplitudes of the left and right traveling pressure waves in domain ① and can be calculated by using the multi-microphone method [13]. Although this method is proposed for experimental studies, it is completely applicable in numerical models as well. To read the pressure values, we define several pressure probes along the z-axis in domain ① of our numerical model and perform the pressure decomposition based on these readings.

3. Numerical Model

We build our numerical model in LMS Virtual.Lab® [14] based on the impedance configuration shown in Figure 1a. The schematic description of the model is given in more detail in Figure 2. The acoustic domains ① and ② are modeled by Eq. (1); the inlet Ω_P is the imposed pressure boundary, and the f-MPP is a combination of the imposed transfer impedance boundary Ω_{Z_t} and vibro-acoustic coupling boundary Ω_S that need to satisfy Eqs. (3) and (4). The remaining boundaries are defined as the sound-hard boundary, Ω_{Z_∞}.

Please note that, although Figure 2 illustrates 2D drawings for the sake of simplicity, the model we describe in this study is built in 3D.

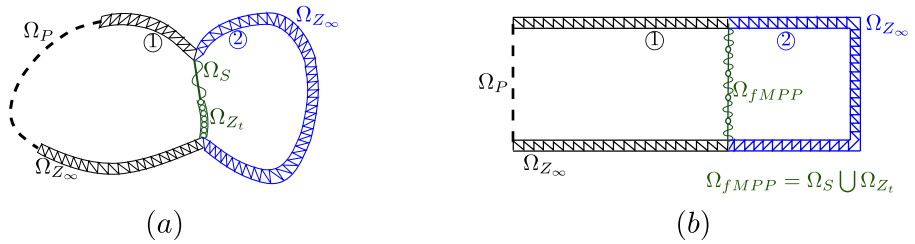

Figure 2: Schematic representation of the numerical model investigated in this study: (a) general geometry for a coupled vibro-acoustic model; (b) impedance tube configuration.

3.1 Finite Element Model for the Coupled System

Writing Eqs. (1) and (2) in weak form, choosing appropriate shape functions and implementing the coupling equations given in Eq. (4), we obtain the set of equations for the coupled system:

$$\left\{ \begin{bmatrix} \mathbf{K}_s & \mathbf{K}_c \\ 0 & \mathbf{K}_a \end{bmatrix} + j\omega \begin{bmatrix} \mathbf{C}_s & 0 \\ 0 & \mathbf{C}_a \end{bmatrix} - \omega^2 \begin{bmatrix} \mathbf{M}_s & 0 \\ \mathbf{M}_c & \mathbf{M}_a \end{bmatrix} \right\} \begin{Bmatrix} \mathbf{w}_u \\ \mathbf{p}_u \end{Bmatrix} = \begin{Bmatrix} \mathbf{F}_{si} \\ \mathbf{F}_{ai} \end{Bmatrix}, \tag{5}$$

where $\mathbf{K}$ is the stiffness, $\mathbf{M}$ is the mass, $\mathbf{C}$ is the dissipation and $\mathbf{F}$ is the forcing matrix. The subscripts 'a', 's' and 'c' represent the words *acoustic*, *structural* and *coupling*. The vectors $\mathbf{w}_u$ and $\mathbf{p}_u$ represent the unconstrained plate displacement and acoustic pressure vectors that need to be solved for. The stiffness coupling matrix $\mathbf{K}_c$ relates the acoustic pressure to plate acceleration; and the coupled mass matrix $\mathbf{M}_c$ relates the acoustic pressure to the plate displacement. The forcing matrices $\mathbf{F}_{ai}$ and $\mathbf{F}_{si}$ introduce the prescribed pressure and displacement vectors into the set of equations.

3.2 Numerical Study Cases

We consider two study cases for the validation of the numerical model: (1) Purely acoustic case, (2) vibro-acoustic case. In both cases the configuration is the same as the one in Figure 1a. The differences in the parameter values are described in this section.

3.2.1 Case 1: Purely Acoustic

In this case study, we compare the classical MPP theory with the numerical model we propose. The former one is implemented into the FEM as a boundary condition connecting domains ① and ②. This boundary is modeled as an *imposed transfer impedance relation*, Ω_Z, whose expression is an averaged transfer impedance over the plate, Z_T, as discussed in Secion 2. Thus, we refer to this model as the **lumped model** in the rest of the paper.

By contrast, the proposed model represents the perforations as transfer impedance patches on the whole plate surface. Since this model allows us to treat each perforation separately, it will be referred to as the **discrete model**. The transfer impedance expression for each patch is calculated from the expression given in Eq. (1). Nevertheless, since the solution of the Helmholtz equation already includes the effect of the area change in the acoustic domains, the last term $(j\delta\omega\rho_0\frac{d_p}{2})$ should be omitted to prevent excess reactance. For the resistive end-correction term $(2\alpha R_s)$, this does not apply due to the fact that Helmholtz equation does not include viscous terms.

For the purely acoustic case, the MPP is not flexible. As a result the entire plate except for the transfer impedance patches is modeled as a *sound-hard boundary*, Ω_{Z_∞}.

3.2.2 Case 2: Vibro-Acoustic

The parameters for this case study are taken from Toyoda *et al.* [6] to be able to compare to their measurements. The coupling in the vibro-acoustic models is achieved through defining the

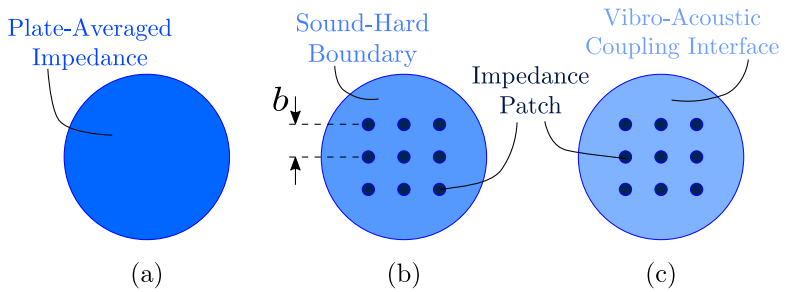

Figure 3: Boundaries connecting domains ① and ②: (a) boundary for the lumped model, (b) boundary for the purely acoustic discrete model, (c) boundary for the vibro-acoustic discrete model.

boundary between domains ① and ② as the *vibro-acoustic coupling interface*, Ω_S. Furthermore, the perforations are modeled as local impedance patches on this flexible boundary, hence the vibro-acoustic models are also discrete models as shown in Figure 3c. To define the flexibility of Ω_S, additional structural parameters such as Young's modulus, Poisson ratio and the loss factor of the flexible plate are needed for this case study.

All the models and their describing properties are given in Table 1.

Table 1: Model parameters.

Parameter	**Model 1A**	**Model 1B**	**Model 2A**	**Model 2B**	**Model 2C**
d_p [mm]	0.20	0.20	N/A	0.5	2.0
t_p [mm]	0.20	0.20	0.50	0.50	0.50
b [1] [mm]	2.5	2.5	10	10	10
n_p [2] [-]	1	9	0	69	69
σ [-]	0.5%	0.5 %	0%	0.2%	2.8%
D [mm]	2.82	8.46	100	100	100
L_1 [mm]	8.46	25.4	300	300	300
L_2 [mm]	60	60	50	50	50
E [N/m^2]	N/A		3×10^9		
η [-]	N/A		0.03		
ν [-]	N/A		0.3		

4. Results and Discussions

For the validation of the purely acoustic case, we first compare the absorption coefficient values given by the discrete model proposed in this paper, lumped model based on the study by Maa [1] and the experiment results from his study. Secondly, we compare the effect of number of perforations in our discrete model. These comparisons are performed in the frequency span of $200\,\text{Hz}<f<2000\,\text{Hz}$.

As show in Figure 4a, if the boundary condition expression is not corrected for the reactive end-correction, we observe discrepancies in the absorption coefficient values. When this correction is performed, the discrepancy between the lumped model and the detailed model decreases significantly. Additionally, Figure 4b shows that the number of perforations is not an important factor with the given

[1] Distance between two neighboring perforations.
[2] Number of perforations.

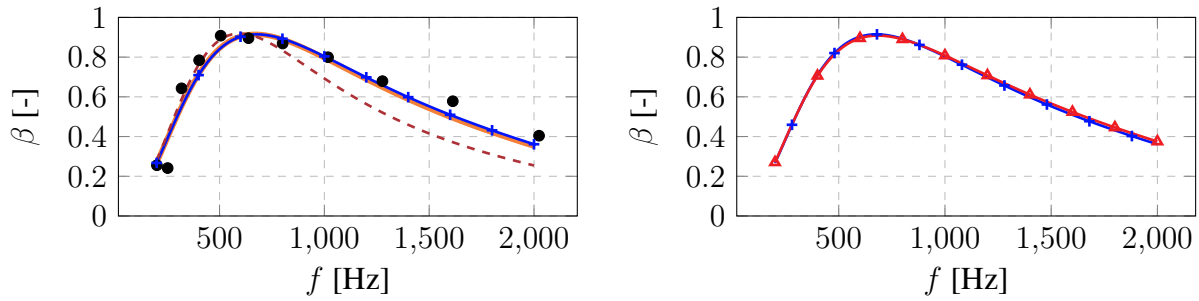

(a) Verification of Model 1A.

(b) Comparison between Model 1A and 1B.

Figure 4: Verifying the proposed discrete model: (a) comparing the model with experiments by Maa [1]; (b) investigating the effect of number of perforations in the model. (•): experiment Data; (—): lumped model; (– –): detailed model with excess reactance; (—+—): discrete model with correction[1 perforation]; (—▲—): discrete model with correction[9 perforations].

value of b, which is the distance between two neighboring perforations. In conclusion, the proposed discrete model represents the purely acoustic case fairly well.

In Case 2, we compare our results with the experiments by Toyoda *et al.* [6]. The parameters defining models 2A, 2B and 2C are taken from their study and used for building the vibro-acoustic model. We compare the results from our numerical model with their experiments in Figure 5.

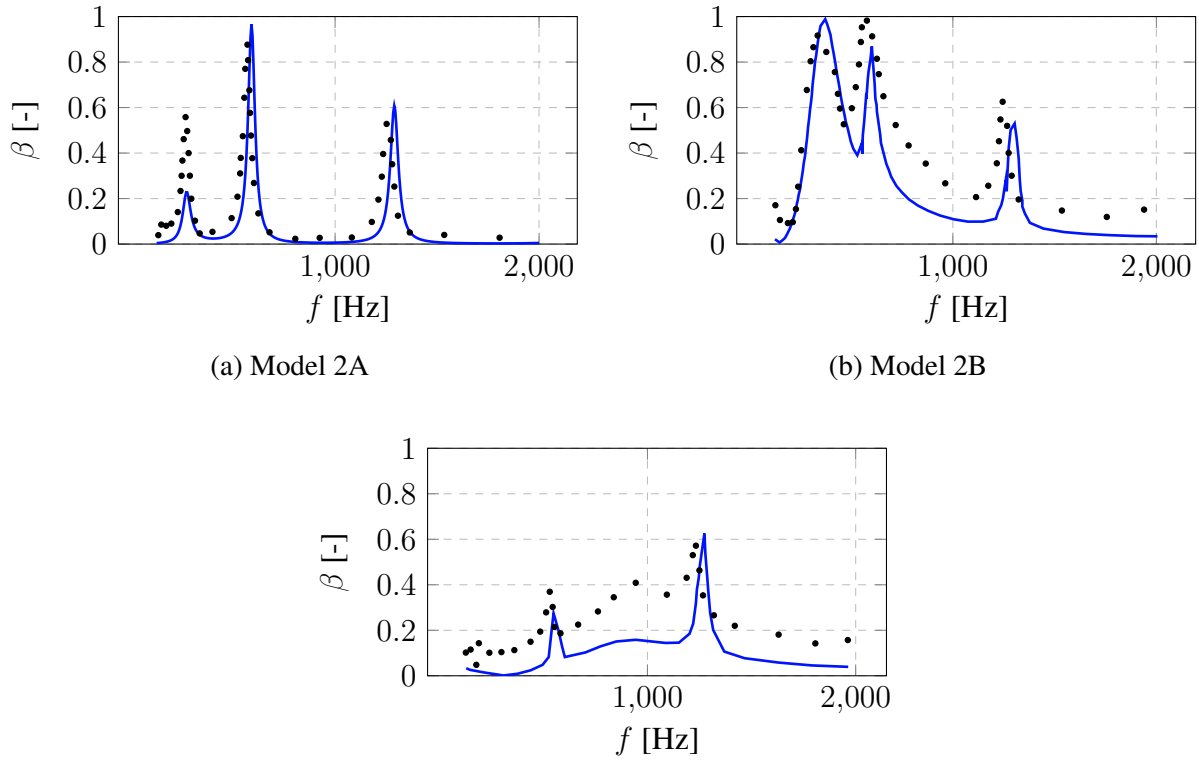

(a) Model 2A

(b) Model 2B

(c) Model 2C

Figure 5: Verification of Case 2 (vibro-acoustic coupling): (—): discrete model; (•): experiment data by Toyoda *et al.* [6].

In Figure 5, we observe two structural and one absorption peaks. The acoustic one changes drastically with respect to the perforation size, but the structural ones are not influenced by that. Toyoda *et al.* report that the 2nd and 3rd eigenfrequencies of the flexible plate are 560 Hz and 1255 Hz [6]. As it can be seen in Figure 5a, the proposed discrete model captures these peaks successfully.

In Figures 5b and 5c, except for the structural peaks, the model underestimates the absorption coefficient measured experimentally. Toyoda *et al.* explains this discrepancy with the presence of *surface admittance* [6, 15] and our discrete model can be improved to capture this effect in the future.

To see if the surface impedance is the only effect responsible of the discrepancies in Figures 5b and 5c, we run simulations with models 2B and 2C in Case 1 and compare the results with the lumped version of these models. Figure 6 shows the results of these extra simulations.

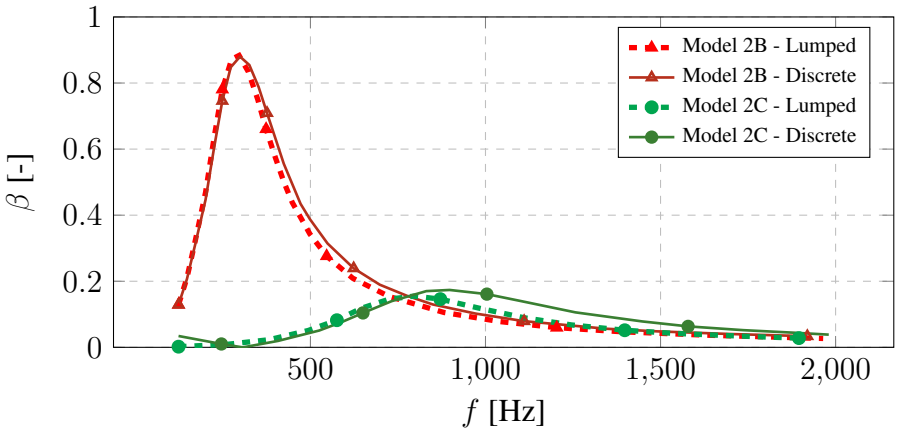

Figure 6: Discrepancy between the lumped and discrete models as the perforation diameter increases.

The comparison of discrete models 2B and 2C with their lumped version shows us there can be an additional source of discrepancy observed in Figures 5b and 5c. As it can be seen in Fig. 6, there is a larger difference between the discrete and lumped models for the model with the larger diameter. We consider this as an implication of the imperfect reactive end-correction. Further study is planned to investigate this issue.

5. Conclusions

This study proposes an efficient numerical model that couples the vibration characteristics of a flexible micro-perforated plate with the acoustics of a fluid domain. Since this model solves the Helmholtz equation for the acoustic part, we introduce the viscous effects as local impedance patches on the flexible plate boundary. As a result of this hybrid approach, the computation time is significantly lower than models solving the Navier-Stokes equations in the entire domain.

In our simulations, we observe a discrepancy between the lumped and discrete models that depends on the perforation diameter. Although omitting the reactive end-correction term helps reducing this difference notably, it does not completely eliminate it. Further study addressing reactive end-correction term is planned.

The proposed discrete model captures the vibro-acoustic system response satisfactorily, especially at the absorption coefficient peaks. Nevertheless, in the rest of the frequency span of interest, there is a slight underestimation of the absorption coefficient value compared to the measurement data. This is another aspect in which our model can be improved.

With this proposed discrete model, it is possible to calculate the sound absorption of f-MPPs whose perforations are not uniformly distributed. It is also possible to model the acoustic characteristics of f-MPPs that have perforations of different size on the same plate. Thus, this approach is a promising tool for parametric studies to optimize the sound absorption of f-MPPs.

Acknowledgments

The presented work is part of the Marie Curie Initial Training Network Thermo-acoustic and aero-acoustic nonlinearities in green combustors with orifice structures (TANGO). We gratefully ac-

knowledge the financial support from the European Commission under call FP7-PEOPLE-ITN-2012.

REFERENCES

1. Maa, D.-Y. Potential of microperforated panel absorber, *Journal of Acoustic Society of America*, **104**(5), 2861–2866, (1998).

2. Temiz, M.A., Lopez Arteaga, I., Efraimsson, G., Åbom, M., Hirschberg, A. The Influence of Edge Geometry on End-Correction Coefficients in Micro Perforated Plates, *Journal of Acoustic Society of America*, **138**(6), 3668–3677, (2015).

3. Temiz, M.A., Tournadre, J., Lopez Arteaga, I., Hirschberg, A. Non-linear acoustic transfer impedance of micro-perforated plates with circular orifices, *Journal of Sound and Vibration*, **366**, 418–428, (2015).

4. Lee, J., Swenson G.W. Compact sound absorbers for low frequencies, *Noise Control Engineering Journal*, **38**(3), 109–117, (1992).

5. Lee, Y.Y., Lee, E.W.M., Ng, C.F. Sound absorption of a finite flexible micro-perofrated panel backed by an air cavity, *Journal of Sound and Vibration*, **287**, 227–243, (2005).

6. Toyoda, M., Mu, R.L., Takahashi, D. Relationship between Helmholtz-resonance absorption and panel-type absorption infinite flexible microperforated-panel absorbers, *Applied Acoustics*, **71**(4), 315–320, (2010).

7. Zheng, W., Huang Q., Li, S., Guo Z. Sound Absorption of Hybrid Passive-Active System Using Finite Flexible Micro-Perforated Panels, *Journal of Low Frequency Noise, Vibration and Active Control*, **30**(4), 313–328, (2011).

8. Bravo, T., Maury, C., Pinhède, D. Sound absorption and transmission through flexible micro-perforated panels backed by an air layer and a thin plate, *The Journal of Acoustic Society of America*, **131**(5), 3853–3863, (2012).

9. Bravo, T., Maury, C., Pinhède, D. Enhancing sound absorption and transmission throgh flexible multi-layer micro-perforated structures, *The Journal of Acoustic Society of America*, **134**(5), 3663–3673, (2013).

10. Li, C., Cazzolato, B., Zander, A. Acoustic impedance of micro perforated membranes: Velocity continuity condition at the perforation boundary, *The Journal of Acoustic Society of America*, **139**(1), 93–103, (2016).

11. Kinsler, L.E., Frey A.R, Coppens A.B. Sanders J.V., *Fundementals of Acoustics*, John Wiley & Sons, New York, USA (2000).

12. Kirchhoff, G. Über das Gleichgewicht und die Bewegung einer elastischen Scheibe, *Journal für die reine und angewandte Mathematik*, **40**, 51–88, (1850).

13. Jang, S., Ih, J. On the multiple microphone method for measuring in-duct acoustic properties in the presence of mean flow, *The Journal of Acoustic Society of America*, **103**(3), 1520–1526, (1998).

14. Siemens PLM Software, LMS Virtual.Lab 13.1, `https://www.plm.automation.siemens.com/en_us/products/lms/virtual-lab/`, (2014).

15. Takahashi, D., Tanaka, M. Flexural vibration of perforated plates and porous elastic materials under acoustic loading, *The Journal of Acoustic Society of America*, **112**, 1456–1464, (2002).